ACS APPLIED MATERIALS & INTERFACES

www.acsami.org

Research Article

Wearable Flexible Perspiration Biosensors Using Laser-Induced Graphene and Polymeric Tape Microfluidics

Nate T. Garland, Jacob Schmieder, Zachary T. Johnson, Robert G. Hjort, Bolin Chen, Cole Andersen, Delaney Sanborn, Gabriel Kjeldgaard, Cicero C. Pola, Jingzhe Li, Carmen Gomes, Emily A. Smith, Hector Angus, Jacob Meyer, and Jonathan C. Claussen*

Cite This: *ACS Appl. Mater. Interfaces* 2023, 15, 38201−38213

Read Online

ACCESS | Metrics & More | Article Recommendations | Supporting Information

ABSTRACT: Wearable biosensors promise real-time measurements of chemicals in human sweat, with the potential for dramatic improvements in medical diagnostics and athletic performance through continuous metabolite and electrolyte monitoring. However, sweat sensing is still in its infancy, and questions remain about whether sweat can be used for medical purposes. Wearable sensors are focused on proof-of-concept designs that are not scalable for multisubject trials, which could elucidate the utility of sweat sensing for health monitoring. Moreover, many wearable sensors do not include the microfluidics necessary to protect and channel consistent and clean sweat volumes to the sensor surface or are not designed to be disposable to prevent sensor biofouling and inaccuracies due to repeated use. Hence, there is a need to produce low-cost and single-use wearable sensors with integrated microfluidics to ensure reliable sweat sensing. Herein, we demonstrate the convergence of laser-induced graphene (LIG) based sensors with soft tape polymeric microfluidics to quantify both sweat metabolites (glucose and lactate) and electrolytes (sodium) for potential hydration and fatigue monitoring. Distinct LIG-electrodes were functionalized with glucose oxidase and lactate oxidase for selective sensing of glucose and lactate across physiological ranges found in sweat with sensitivities of 26.2 and 2.47 × 10^{-3} μA mM^{-1} cm^{-2}, detection limits of 8 and 220 μM, and linear response ranges of 0−1 mM and 0−32 mM, respectively. LIG-electrodes functionalized with a sodium-ion-selective membrane displayed Nernstian sensitivity of 58.8 mV $decade^{-1}$ and a linear response over the physiological range in sweat (10−100 mM). The sensors were tested in a simulated sweating skin microfluidic system and on-body during cycling tests in a multisubject trial. Results demonstrate the utility of LIG integrated with microfluidics for real-time, continuous measurements of biological analytes in sweat and help pave the way for the development of personalized wearable diagnostic tools.

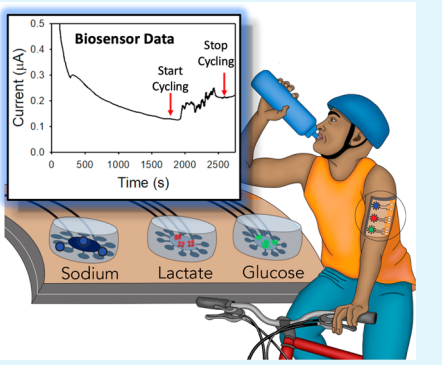

KEYWORDS: *Graphene, sweat, wearable sensor, flexible sensor, metabolites, electrolytes*

INTRODUCTION

The field of wearable or on-body sensing promises non-invasive, real-time health monitoring that can provide insight into dynamic physiological phenomena.[1,2] Current commercialized devices such as Fitbit and Apple Watch provide continuous measurement of physiological conditions, including heart rate, pulse oximetry, and movement, but they lack the capability to sense biochemical information. Daily health tracking, continuous stress measurement, and physical activity quantification demand on-body continuous sensors to provide meaningful data as the type, intensity, and duration of active and resting states change throughout the day. In particular, the chemical monitoring of bodily fluids has expanded rapidly with reports of sensors for saliva, tears, blood, and perspiration.[1−3] Perspiration or sweat represents an appealing sensing medium due to a wide variety of biomedically relevant analytes found within and amenability to noninvasive, facile sampling, which is in sharp contrast to the pain and cumbersome nature of acquiring blood or even subcutaneous fluid samples.

Colorimetric and electrochemical sensors are the most common on-body sensing modalities for sweat monitoring. Early works by Gao et al.[4] as well as from Rogers and co-workers[5,6] demonstrated wearable bands of sensors and polydimethylsiloxane (PDMS) microfluidics with integrated colorimetric sensing of glucose. While colorimetric detection represents a low-cost method of gauging concentrations, it is limited to single measurements (based on the irreversible colorimetric reaction), requires complex microfluidics to allow for time-gated sampling,[7] and is often subject to interpretation error of color hue or intensity. However, wearable, electro-

Received: April 3, 2023
Accepted: July 13, 2023
Published: August 1, 2023

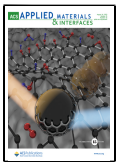

chemical sensors offer a promising alternative as they can continuously measure quantitative concentrations of analytes with easy-to-read digital readouts.[8] Numerous wearable electrochemical sensors have been created to monitor metabolites and electrolytes in sweat including smart wristbands, temporary tattoos, eyeglasses, socks, gloves, and headbands.[9] However, such devices typically require the use of complex/expensive materials or complex manufacturing techniques (e.g., fabrication of nanowires, printing of multiple solution-phase inks, and use of noble metals such as platinum and gold). Moreover, such devices generally do not contain appropriate microfluidics that are needed to acquire ample, consistent, and clean volumes of sweat for accurate analysis. Wearable sweat sensors that do not utilize microfluidics often suffer from challenges associated with liquid evaporation and low-sweat volumes due to the inability to concentrate and channel sweat to the sensor surface rapidly, irregular sweat volumes or mixing of old and new volumes due to changes in exercise that cannot be metered or channeled to the sensor, and contamination from the environment as the sensor is exposed to ambient conditions.[10] A more low-cost, high-throughput manufacturing of wearable sensors would also increase sensor accuracy as sensors could be disposed after a single use in lieu of repeatedly using the sensor, which leads to biofouling and inaccurate readings. Furthermore, high-throughput manufacturing of wearable sensors would enable the operation of large-scale multisubject trails that are desperately needed to elucidate the connection between sweat biomolecules and human health.[11]

One of the more promising routes toward low-cost high-throughput wearable electrochemical sensors are those based on carbon-nanomaterial based biosensors.[1,2] Flexible carbon nanomaterial sensors offer a low-cost, facile fabrication scheme toward producing sensors at industrial scale for electrochemical sensing. Such carbon nanomaterial sensors can also be fabricated without precious metals such as gold and platinum, hence are lower-cost than conventional electrodes and are consequently more amenable for use in disposable single-use sensors. Graphene[12] and carbon nanotube (CNT)[13] based sensors have been studied, with various fabrication methods available including producing high quality thin film graphene and CNTs via chemical vapor deposition (CVD). However, CVD is a high-temperature vacuum process that is low-yielding, and hence expensive. Other methods like inkjet[14] or aerosol printing[15] are more cost-effective as they print graphene inks obtained from liquid-phase exfoliation of graphite, which can be performed using large batch processing techniques. However, these techniques still require ink formulation, printing, and annealing steps that encumber the electrode manufacturing process. A promising alternative to these printing techniques is the laser-induced graphene (LIG) technique, which converts nonconductive polyimide into conductive sp^2 hybridized carbon or graphene through the applied, concentrated energy of a laser engraver (e.g., CO_2 laser cutter).[16] The laser engraver synthesizes and patterns graphene sensors in a single step through a direct-write process, while avoiding the need for any chemical processing. The resulting LIG also exhibits high surface area and is porous with a high density of edge plane sites, which are beneficial for biofunctionalization and heterogeneous charge transport during electrochemical sensing.[17] These positive attributes have propelled the burgeoning growth of LIG-based electrochemical sensors in a wide variety of fields including environmental monitoring,[18] foodborne pathogen detection,[19] and medical diagnostics.[20]

LIG-based electrochemical sensors for multianalyte detection in perspiration are beginning to emerge. For example, an LIG-based wearable electrochemical sensor was used for acid/tyrosine and uric acid for monitoring gout/metabolic disease and for sensing cortisol for stress monitoring.[21,22] This latter research by Gao and co-workers combined microfluidics with sensors and completed a pilot human study that was able to monitor the diurnal cycle and stress-response profile of sweat cortisol. In terms of multianalyte monitoring of metabolites and electrolytes, LIG-based sensors have been more limited. For example, LIG-based electrodes have been modified with gold and platinum nanoparticles for measuring sweat biomarkers including glucose and pH monitoring.[23] However, this sensor did not incorporate fluidics into the design, nor did it include on-body testing. Recently researchers have combined electrolyte (i.e., potassium) and metabolite (glucose and lactate) LIG-based sensors onto a wearable device with promising results.[24] However, this sensor lacked microfluidics and was tested only on a chicken leg without actual testing on humans. Also, recent progress has demonstrated that LIG-based electrochemical biosensors and open microfluidics can be created on a single flexible polyimide swatch for multianalyte environmental monitoring, but such open microfluidics would not be able to retain and channel fluid during body movement, nor would it protect sweat from environmental contamination.[25]

In this study, we introduce carbon-based wearable biosensors combined with a closed polymeric microfluidic patch for continuous, real-time monitoring of sweat glucose, lactate, and sodium. The real-time sensing of metabolites such as glucose and lactate and electrolytes such as sodium has become a major focus for on-body wearable sensing and provides numerous benefits regarding the ability to gain information about an individual's physiology (see Supporting Information). The flexible sensors are developed with LIG coupled with medical tape microfluidics to allow for conformal, on-body sensing that enables single-use sensing due to the high-throughput manufacturability of both the sensors and the microfluidics. The sensors are initially tested *ex vivo* on a microfluidic device that delivers artificial perspiration with added target biomarkers to the sensors via laser-drilled holes of size and distribution similar to those of human skin pores. After this initial testing and characterization, the sensors are tested on-body during cycling tests in a multisubject trial with 15 participants of varying sex, age, weight, and fitness level. The glucose, lactate, and sodium sensors show consistent sensitivity across physiological ranges found in perspiration. The use of scalable manufacturing techniques to create the graphene-based sensors (i.e., utilization of laser-induced graphene) and polymeric microfluidics (i.e., thin film polyethylene terephthalate (PET) combined with medical tape) presents a unique cost-effective platform for flexible form fitting sensors. Hence, this work develops a single-use biosensor patch that has the potential for wide scale use to help decode the utility of sweat for medical diagnostics and real-time health monitoring.

RESULTS AND DISCUSSION

Laser-Induced Graphene (LIG) Sensor Fabrication and Material Characterization. LIG sensors were fabricated by first photonically annealing polyimide sheets with a CO_2

https://doi.org/10.1021/acsami.3c04665
ACS Appl. Mater. Interfaces 2023, 15, 38201−38213

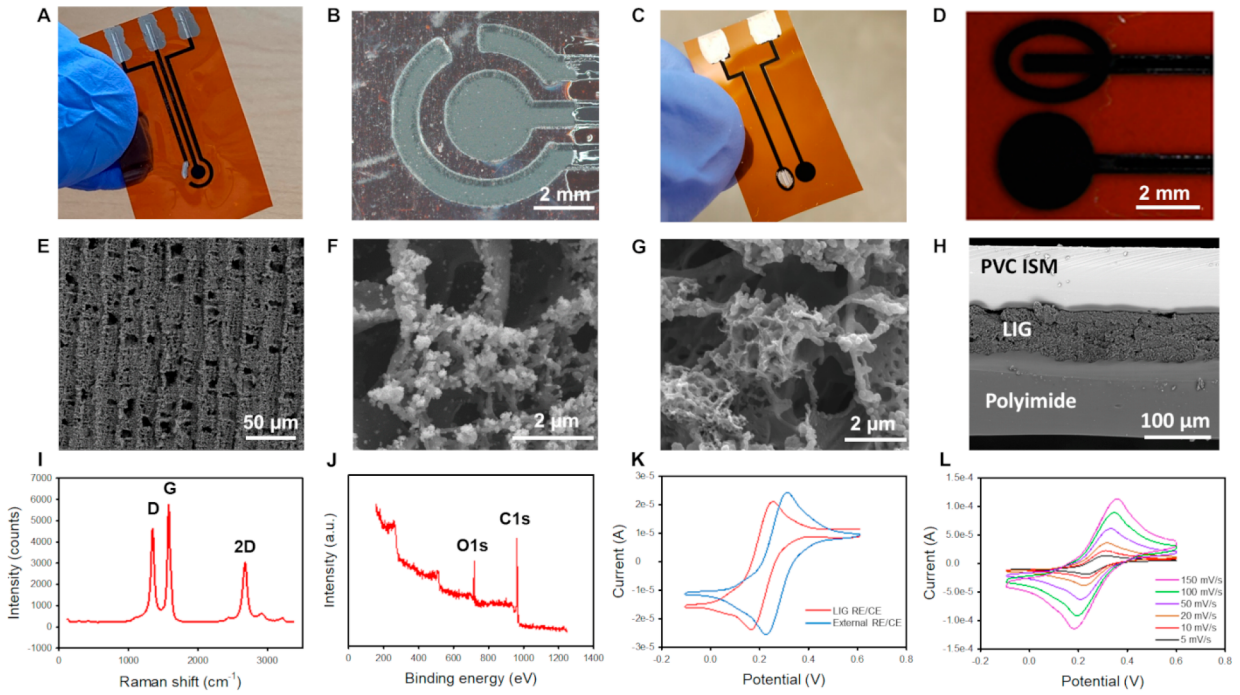

Figure 1. Laser-induced graphene (LIG) fabrication, biofunctionalization, and initial characterization. (A) Image of an amperometric LIG sensor with Ag leads and a Ag/AgCl reference electrode. (B) Microscopic image showing bare LIG working, reference, and counter electrodes along with a passivation layer protecting the LIG electrical leads. (C) Image of LIG ion selective electrode (ISE) with Ag leads and a Ag/Cl reference electrode. (D) Close-up image of LIG ISE. (E) Scanning electron microscopy (SEM) image of LIG showing laser rastering pattern and disordered edges. (F) SEM image of platinum nanoparticles on LIG, with particle formation primarily on LIG edges. (G) SEM image of tetrathiafulvalene (TTF) deposited on LIG. (H) SEM of LIG ISE cross section showing stacked layers of polyimide, LIG, and a PVC ion selective membrane (ISM). (I) Raman spectrum of LIG, showing the characteristic D, G, and 2D peaks. The spectrum displayed is the average spectrum for 18 random locations across a 1 cm^2 LIG sample. (J) Full survey X-ray photoelectron spectroscopy (XPS) of bare LIG showed peaks for carbon and oxygen. (K) Cyclic voltammograms (CVs) comparing the fabricated LIG reference electrode/counter electrode and the external silver/silver chloride liquid junction reference electrode/platinum wire counter electrode. (L) CVs of bare LIG in ferri-/ferrocyanide redox probe at scan rates ranging from 5 to 150 mV/s.

laser at controlled focal length, power, rastering speed, and frequency. The laser path was controlled by software to produce LIG in the shape of a 3-electrode design for amperometric sensing (Figure 1A,B,E,F) or 2-electrode design for ISEs (Figure 1C,D,G,H) using all LIG based electrodes. The working, reference, and counter electrodes were shaped and sized to fit inside microfluidic patches (circular sensing chamber with an 8-mm diameter for ISEs, and a 5.5-mm diameter for enzyme sensors). Laser power, speed, and frequency (7%, 7%, 50%) settings were tuned according to the CO_2 laser settings (see Experimental Section). Silver/silver chloride (Ag/AgCl) paste was applied to the LIG reference electrode to generate a fixed potential, and the LIG counter electrode was left bare. The electrode stem was passivated with fast-drying acrylic polish to avoid short-circuiting in liquids, and potentiostat attachment points (i.e., electrical contact pads) were coated with silver paste to improve the conductivity and mitigate wear (Figure 1A).

The material properties of the developed LIG were evaluated before subsequent biofunctionalization and testing. The Raman spectra of the LIG displayed characteristic D, G, and 2D peaks associated with turbostratic, multilayer graphene (Figure 1I).[26,27] The D peak at around 1350 cm^{-1} is indicative of defects in graphene, and the G peak at around 1580 cm^{-1} is assigned to the bond stretching from all pairs of sp^2 carbon atoms.[27,28] The calculated I_D/I_G ratio of 0.8 ± 0.3 indicates high disorder and heterogeneity in the LIG. The 2D peak at around 2690 cm^{-1} results from the second order zone-boundary phonons, and the calculated I_{2D}/I_G ratio 0.52 ± 0.05 suggests multilayer graphene structures.[29,30] The ferri-/ferrocyanide redox complex is known to be sensitive to surface oxides on carbon electrodes, and the reactions will be significantly hindered in the absence of oxides.[31] Our observed relatively fast electron transfer rates and remaining O_2 groups measured by X-ray photoelectron spectroscopy (XPS) demonstrate the importance of such surface oxides on the LIG electrodes (Figure 1J). Scanning electron microscopy (SEM) imaging reveals the three-dimensional, rough, and porous structure of the fabricated LIG (Figure 1E−G). Such structural characteristics result in a device with a high surface area, which is desirable for electrochemical reactions.[19]

Next, the electrochemical behavior of the LIG was analyzed. First, the capability of the LIG-based counter electrode and solid-state Ag/AgCl reference electrodes (Figure 1K) was compared to an external platinum wire and Ag/AgCl liquid junction reference electrode. In both test scenarios, the developed LIG was used as the working electrode. Cyclic voltammograms (CV) acquired in a ferro-/ferricyanide solution displayed a slight shift in potential of about 0.05 V. This shift is related to the difference in standard potential of the fabricated solid-state Ag/AgCl reference electrode compared to the liquid junction Ag/AgCl. Aside from this shift, the all-LIG three-electrode setup exhibited a stable signal as the external reference and counter system and were used for all amperometric sensing (LIG used for the ISE reference electrode is discussed later). Next, CVs of the LIG-based

https://doi.org/10.1021/acsami.3c04665
ACS Appl. Mater. Interfaces 2023, 15, 38201−38213

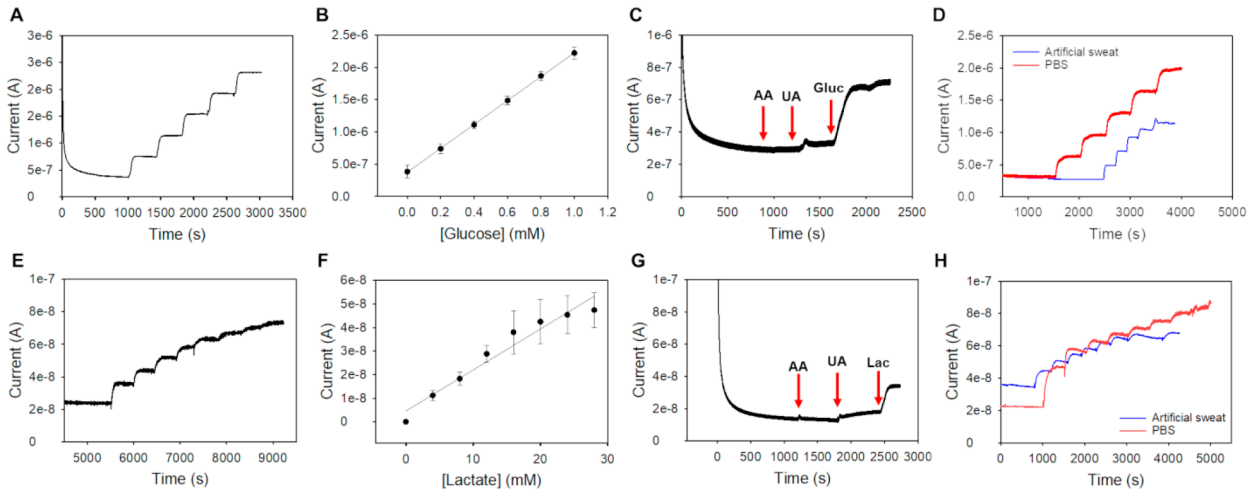

Figure 2. Electrochemical characterization of glucose (A–D) and lactate (E–H) functionalized laser-induced (LIG) biosensors. All tests in pH 7.4 phosphate buffered saline (PBS) (except where noted) and in a stirred beaker. (A) Real-time amperometric response of the LIG glucose biosensor to 0.2 mM glucose additions. (B) Individual glucose sensor dynamic range and repeatability for n = 3 (values presented as average ± standard deviation). (C) Interference tests for ascorbic acid (AA, 500 μM) and uric acid (UA, 100 μM) and subsequent response to glucose (Gluc). (D) Glucose biosensor performance in PBS and artificial sweat using the same LIG glucose biosensor in both tests. (E) Real-time amperometric LIG lactate response to 4 mM lactate additions. (F) Individual lactase sensor dynamic range and repeatability for n = 3 (values presented as average ± standard deviation). (G) Interference tests for AA, UA, and the subsequent response to lactate (Lac). (H) Comparison of the lactate biosensor response in PBS and artificial sweat.

Table 1. Comparison of Glucose Perspiration Sensors with Microfluidics Using the Enzyme Glucose Oxidase (GOx)

electrode material	sensitivity (μA mM^{-1} cm^{-2})	LOD (μM)	linear range (mM)	microfluidics	reference
MXene/methylene blue	2.4[a]	17.05	0.08–1.25	printed wax/paper	37
anisotropic conductive adhesive/gold	15.13 ± 0.8	0.9 ± 0.05	0.0009–0.6	adhesive thin-film	36
gold	2.35[a]	not listed	0–0.2	sensor on skin, covered with polymer band	4
LIG	26.2	8	0.008–1	polyethylene terephthalate/medical adhesive	this work

[a]Legend: μA/mM.

electrodes (Figure 1L) were recorded at different scan rates (5, 10, 20, 50, 100, and 150 mV/s) and were used to estimate the peak oxidation current ($i_{p,ox}$) (2.35 × 10^{-5} A at 10 mV s^{-1}), potential peak separation (ΔE_p) (82 mV at 10 mV s^{-1}), heterogeneous electron rate coefficient (k^0) (1.32 × 10^{-3} ± 1 × 241 10^{-3} cm s^{-1}), and electroactive surface area (ESA) (7.71 × 10^{-2} 242 cm^2). Such electrochemical sensing properties show relatively fast charge transport kinetics and indicate a quasi-reversible electrode transfer behavior.[32]

LIG Glucose Biosensor Fabrication and Initial Characterization. The glucose sensors were developed by first electrochemically depositing a layer of polyphenylenediamine (PPD) onto the LIG-Pt via CV to selectively repel known interferants in sweat, such as ascorbic and uric acid; PPD forms pores over the electrode surface at sizes that allow small molecules like H_2O_2 to pass through but restrict larger molecules, thus eliminating the possibility of oxidizing interferent species (Figure 2C, G).[33] Next, GOx was covalently linked to LIG using ethyl-3-(3-(dimethylamino)propyl) carbodiimide/N-hydroxysuccinimide (EDC/NHS) chemistry (see Experimental Section). It is important to note here that the GOx converts glucose to gluconic acid and H_2O_2 which is decomposed rapidly on the platinum nanoparticles on the LIG surface (~100–200 nm, Figure 1F) as such platinum nanoparticles have shown to improve the electrochemical reactivity of carbon-based electrodes to H_2O_2 during glucose sensing.[34,35] The resulting glucose biosensors exhibited a sensitivity of 26.2 μA mM^{-1} cm^{-2} and a limit of detection of 8 μM over the human physiological range (0–1 mM) when evaluated in vitro (Figure 2A,B). Calibration tests were also conducted in artificial sweat (Figure 2D). The sensitivity was slightly lower in artificial sweat (part D) compared to PBS. This lower sensitivity can be related to the lower pH (from 7.4 to 6.8) and ionic strength of artificial sweat. This sensor exhibited a linear increase in current across the physiological range in human perspiration (0–1 mM) and a sensitivity of 12.6 μA mM^{-1} cm^{-2} and limit of detection (LOD) of 47.7 μM. The sensor also displayed fast response times, reaching 90% of signal in 80 s in PBS. Individual sensor repeatability was also excellent with R^2 = 0.99 and low error bars (sd <1.0 × 10^{-7}) at all concentrations (Figure 2B).

The performance of the developed LIG-based glucose biosensors compared favorably to other wearable glucose sensors previously reported in the literature that use the same GOx enzyme and incorporate some level of microfluidics into the sensor design (Table 1). These published results are promising but have some distinct drawbacks. More specifically, an anisotropic conductive film sensor harnessed mediator technology to selectively detect glucose, but the sensor's linear range did not reach the physiological range of glucose in sweat

https://doi.org/10.1021/acsami.3c04665
ACS Appl. Mater. Interfaces 2023, 15, 38201–38213

Table 2. Comparison of Lactate Perspiration Sensors with Microfluidics That Use Lactate Oxidase (LOx)

electrode material	sensitivity (μA mM^{-1} cm^{-2})	LOD (μM)	linear range (mM)	microfluidics	reference
graft-polymerized MgO-templated carbon	24	300	0.3−50	PDMS	38
Ti (10 nm)/Cu (550 nm)/Ti (20 nm)/Au (200 nm)	29.6	50	4−20	PDMS	39
CNT	10.31	not listed	1−20	GORE-TEX textile	40
LIG	2.47 × 10^{-3}	220	0.22−28	polyethylene terephthalate/medical adhesive	this work

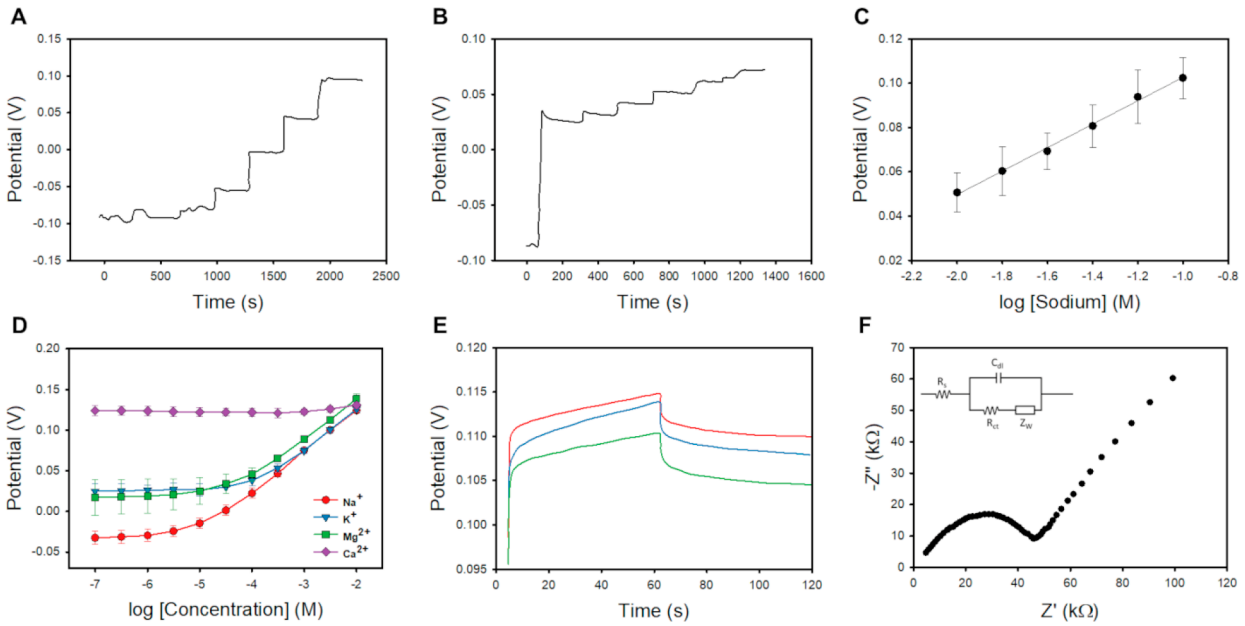

Figure 3. Electrochemical characterization of laser-induced graphene solid contact ion-selective electrodes (LIG SC-ISE). (A) Sensor response in 1 decade intervals of sodium concentration over standard ISE range (10^{-6}−10^{-1} M). (B) Sensor response in 0.2 decade intervals of sodium concentration over a physiological range (0−90 mM). (C) Linear regression of sodium response over physiological range for one electrode tested thrice (average ± standard deviation). (D) Selectivity plots for relevant interfering ions in sweat using the fixed interference method. (E) Chronopotentiometry response for n = 3 sensors. (F) Electrochemical impedance spectroscopy (EIS) response and associated circuit model.

and additionally incorporated multiple expensive noble metals (e.g., silver and gold) to improve the utility of the sensor.[36] A multiplexed biomarker sensor that did incorporate a microfluidic patch to channel and protect sweat for on-body analyte detection was developed but similarly did not meet the physiological range of glucose in sweat and utilized electron-beam evaporated gold, further increasing the cost and complexity of the sensor fabrication.[4] Similarly, a wearable device was integrated onto a sensing paper incorporating MXene and a mediator but only detected glucose and lactate, omitting the benefit of detecting sweat electrolytes.[37]

LIG Lactate Biosensor Fabrication and Initial Characterization. The development of the LIG-based electrochemical lactate biosensor required the use of a mediator in order to achieve linear current response over a physiological range of lactate in sweat (maximum of 32 mM).[6] Briefly, an LIG electrode was functionalized with a solution of the redox mediator tetrathiafulvalene (TTF), which mediates the electron transfer from LOx to the sensor surface (Experimental Section). Subsequent coatings of chitosan, LOx/glutaraldehyde, and PVC were applied to obtain the lactate biosensor on LIG. These lactate biosensors displayed sensitivity even at high concentrations of lactate, likely due to the redox pathway utilizing TTF instead of relying on O_2 limited oxidation of H_2O_2 as is the case with the glucose sensors that utilize an oxidase enzyme (Figure 2). Along with a wide sensing range of 0−28 mM, the lactate biosensors exhibited a sensitivity of 2.47 × 10^{-3} μA mM^{-1} cm^{-2} in PBS and 2.30 × 10^{-3} μA mM^{-1} cm^{-2} in artificial sweat (Figure 2E, H), as well as a detection limit of 220 μM. The developed lactate biosensors displayed high repeatability (sd < 3.0 × 10^{-8}) with slightly more measurement discrepancy at higher concentrations (Figure 2F). Given the additional coating layers needed for the lactate biosensors compared to the developed glucose biosensors, the observed lower sensitivity and slightly higher response time (110 s to reach 90% of signal) was expected. The lactate sensors were selective for lactate, with minimal interference from other electroactive species such as uric and ascorbic acid (100 μM and 500 μM) (Figure 2G). The developed LIG lactate biosensor also compared favorably to other wearable lactate perspiration biosensors that used a similar LOx enzyme as the biorecognition agent and incorporated some level of microfluidics into the sensor design (Table 2). However, like the published glucose biosensors, these lactate biosensors exhibited some distinct drawbacks. For example, a PDMS microfluidic biosensor that incorporated lactate oxidase-functionalized electrodes onto a grafted magnesium oxide surface displayed a wide sensing range but required a complex fabrication scheme with an electron beam irradiation to induce graft polymerization.[38] Other wearable lactate biosensors were

https://doi.org/10.1021/acsami.3c04665
ACS Appl. Mater. Interfaces 2023, 15, 38201−38213

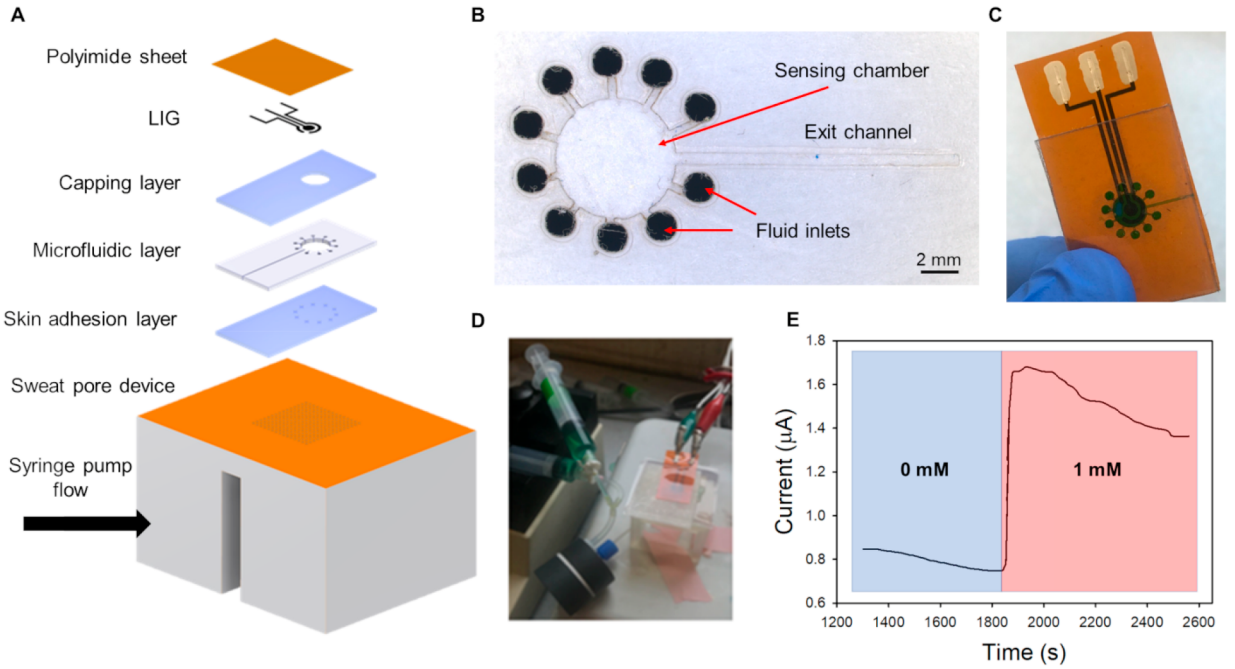

Figure 4. Microfluidic testing overview. (A) Graphical layer level depiction of the laser-induced graphene (LIG) sensor, microfluidics, see Supporting Information, and a simulated skin testing device. (B) Photograph of poly(ethylene terephthalate) (PET) microfluidic channel layer. (C) Photograph of integrated sensor and microfluidic to create the sensor patch. (D) Photograph of sensor and wearable patch on syringe pump simulated sweating device and subsequent (E) response to the flow of artificial perspiration spiked with 1 mM glucose.

unable to monitor lactate concentration up to the 32 mM maximum concentration that can be found in sweat and like the previous example required complex fabrication protocols such as photolithography and metal evaporation to create titanium, copper, and gold circuitry[39] or required the use of expensive carbon nanotubes.[40]

Sodium Solid Contact Ion Selective Electrode Sensor Fabrication and Characterization. Next, the LIG electrodes were functionalized with a sodium ionophore containing a PVC membrane to create a sodium sensing solid contact ion selective electrode (SC-ISE) (Experimental Section). The constructed sodium SC-ISEs were first characterized and calibrated in stirred beaker tests using PBS and artificial sweat (Figure 3A,B). The sensors showed Nernstian sensitivity of 58.8 ± 11.3 mV/decade (n = 5) over ranges typically described for ISEs (10^{-5}–10^{-1} M) as well as over the expected physiological range (10–100 mM). Individual sensor reproducibility was also investigated over the physiological range, presenting consistent linear behavior (Figure 3C). The sensors were selective for sodium with respect to other cations found in sweat and that are known to cause interference with the sodium ionophore. Selectivity coefficients, found using the Nikolskii–Eisenman equation (eq 1), were obtained from fixed interference method tests,

$$E = K + \frac{2.303RT}{z_i F}\log(a_i + K_{i,j}^{POT} a_j^{z_i/z_j}) \quad (1)$$

where E^0 is the standard potential; R is the gas constant; T is the temperature in K; F is the Faradaic constant; z_i is the ionic charge of ion i; z_j is the ionic charge of ion j; a_j is the activity of ion i; and a_j is the activity of ion j. Interferent cations were held at 10 mM, and selectivity coefficients were reported as 0.06, 0.12, and 0.001 for K_{Na^+,K^+}^{POT}, $K_{Na^+,Ca^{2+}}^{POT}$, and $K_{Na^+,Mg^{2+}}^{POT}$, respectively (Figure 3D). Chronopotentiometry (Figure 3E) was also used as a preliminary test, before actual long-term assessments, to study the potential stability of SC-ISE due to polarization.[41] Applying a ± 1 nA current, representing high current conditions relative to the small input current from a high-impedance voltmeter, the potential stability ($\frac{\Delta E}{\Delta t}$) can be related to the capacitance of the SC-ISE (eq 1). For the LIG in this study, the average capacitance observed for sensors was 10.4 ± 1.9 μF, which is higher than values observed for simple coated wire SC-ISEs, but much lower when compared to other carbon-based transducers or even LIG-based ISEs.[41,42] Electrochemical impedance spectroscopy (EIS) is also used to characterize ISE functionality by assessing physical damage, biofouling, and leaching of membrane components.[43] The EIS spectra collected for this study exhibited a high-frequency semicircle where an equivalent circuit model was fitted, resulting in a charge transfer resistance of 41.2 ± 1.24 kΩ. The LIG working electrode was paired with a LIG reference electrode by coating LIG electrodes with Ag/AgCl ink so that the open circuit potential between the two could be measured. Given the high concentration and fluctuation of chloride ions in sweat, sufficient considerations should be taken to ensure interference does not occur when using a solid contact Ag/AgCl reference electrode. Following previous protocols, the LIG Ag/AgCl reference electrode was coated with carbon nanotubes and poly(vinyl butyral) (PVB) to exclude chloride ions from interacting with the underlying reference electrode. All other testing was performed with this modified electrode.[44]

LIG Biosensors Integrated with Tape Microfluidics for Simulated Sweat Testing. Before on-body testing, the LIG sensors were integrated with soft polymeric microfluidics to verify the sensing capability of the three distinct LIG sensors (glucose, lactate, and sodium) across the physiological concentration range in an artificial sweat perspiration background and under flowing conditions. To this end, the fabricated sensors were fitted to tape/polyethylene tereph-

https://doi.org/10.1021/acsami.3c04665
ACS Appl. Mater. Interfaces 2023, 15, 38201–38213

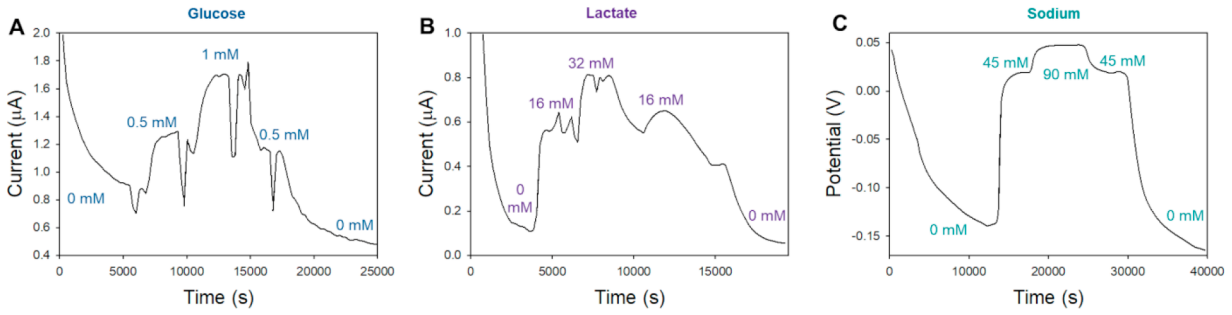

Figure 5. Multiple concentration steps in syringe pump testing of the integrated glucose and lactate laser-induced graphene (LIG) biosensors showing (A) amperometric response to 0, 0.5, and 1 mM glucose solutions, (B) amperometric response to 0, 16, and 32 mM lactate solutions, and (C) potentiometric response 0, 45, and 90 mM sodium solutions.

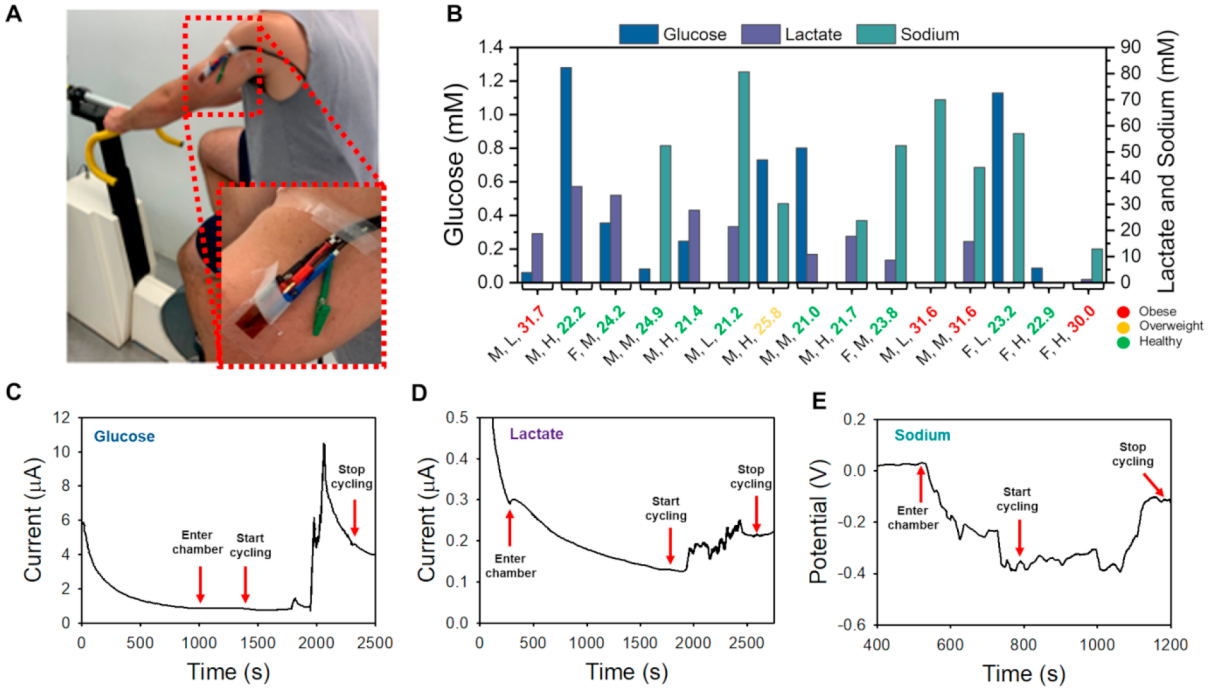

Figure 6. Integrated microfluidic LIG sensor patches used during on-body cycling tests. (A) Photograph of experimental setup including participant, sensor, and microfluidic patch, and stationary cycle. Inset: photograph of sensing patch. (B) Actual concentration of glucose, lactate, and sodium obtained from the Iowa State Metabalomics Lab and sodium assay kit with data labels indicating gender, physical activity level (Low, Medium, High), and BMI. The data presented here was obtained from the IRB approved study. (C) LIG GOx sensor response during cycling. (D) LIG LOx sensor response during cycling. (E) LIG sodium ISE response during cycling.

thalate (PET) microfluidics (Figure 4A) and exposed to flowing artificial sweat (0 mM glucose) and a separate solution spiked with glucose to reach a concentration of 1 mM (see Experimental Section). The experimental goal was to observe sensor performance under constant amperometric monitoring and to obtain relative current plateaus under 0 and 1 mM flowing conditions. The adhesion of the microfluidic device to the perspiration pore layer was important to force fluid flow inside and through the microfluidics system and prevent leaking underneath the microfluidics. Due to the flexibility of the constructed sensor and microfluidic patch, watertight sealing and flow of fluid was achieved through the inlets, sensing chamber, and out the exit channel (Figure 4C). Once the device was attached, artificial sweat with no added glucose was used to fill the volume of the perspiration pore device (350 μL in volume) and microfluidic patch. The sensor was connected to the potentiostat, a potential of +0.6 V vs Ag/AgCl was applied, and current was measured at the GOx functionalized working electrode (Figure 4D). Once again, capacitive current drain was observed, and as the syringe pump continued to flow perspiration through the device (visually confirmed by observation of a growing droplet at the exit channel of the microfluidics), a relative plateau was reached. The current value (μA) was slightly elevated from the plateau observed in the stirred beaker testing most likely due to the enhanced mass transport of target analyte to the biosensor surface due to the forced convection created by the microfluidic.[45] Once the sensor was loaded and fluid was observed to flow through the device, the syringe was exchanged for 1 mM glucose spiked artificial perspiration, and flow was continued at the same rate. Therefore, an increase in current was expected once the glucose-free fluid inside the sensing chamber of the microfluidic patch was replaced with glucose rich fluid (glucose concentration of 1 mM) (Figure 4E). As a demonstration of the fluidic refreshing efficiency of the microfluidic channel design, a sharp increase

https://doi.org/10.1021/acsami.3c04665
ACS Appl. Mater. Interfaces 2023, 15, 38201−38213

in current was observed, reaching a maximum value in ∼30 s. This increase in current then drifted slightly negative, likely caused by the formation of a diffusion layer in the laminar flow conditions inside the microfluidics. Comparison of the change in current plateaus at 0 and 1 mM with values obtained in stirred beaker tests were largely in agreement, but the discrepancy suggests that issues such as variable perspiration rate or stationary fluid inside the microfluidics need to be accounted for in determining an accurate representation of perspiration analytes. The same test was performed using the LOx and sodium ISE sensors, with a potential of +0.4 V vs Ag/AgCl applied and spiked perspiration solutions of 0 and 32 mM lactate and open circuit potential and spike perspiration solutions of 0 and 90 mM sodium used in place of glucose (data not shown). Similar observations were noted with the sensor reaching an initial plateau, rising to a higher value in response to 32 mM lactate fluid reaching the sensing chamber, and then returning to the 0 mM value upon flow of a 0 mM solution.

Next, the sensors were exposed to varying target analyte concentrations (0, 0.5, and 1 mM glucose solutions; 0, 16, 32 mM lactate solutions; 0, 45, and 90 mM sodium solutions) while testing with the microfluidics (Figure 5). The same procedure was used as before, with an additional concentration step used halfway through the range for each sensor. Even over these larger time scales, both sensors displayed good adherence to previous midpoint values (16 mM and 0.5 mM) indicating low sensor and fluidic patch hysteresis. Some drift in 0 mM signal was observed for both sensors, but given the long duration of this experiment and the artificially low concentrations, which would not occur in human sweat, the sensor performance appears to be highly functional. In long-term drift tests under flowing conditions, the enzymatic sensors exhibited minimal change in current over 12 h (1.06×10^{-8} A h^{-1}). This demonstrates the robustness of this system for long-term wear cases, both with respect to the electrochemical functionality of the LIG and attached enzyme as well as the mechanical and fluidic pressure requirements of the tape/PET microfluidics.

On-Body Cycling Tests with the LIG Sensors Integrated with Tape Microfluidics. To test the sensor and patch system in a real-world case, devices were fabricated, calibrated, and tested on-body cycling tests in a multisubject trial with 15 participants of varying sex, age, weight, and fitness levels exercising on a stationary bicycle (see Supporting Information). To begin the experiment, the skin surface of each subject was cleaned using an alcohol swab, and the sensing patch was applied. Prior to sensor application, the internal sensing chamber was filled with PBS to eliminate large initial fluctuations in signal due to limited or nonexistent fluidic contact of the electrodes. Once the initial signal stabilized, the effects of sweating and cycling at a low intensity were investigated (Figure 6). Initial on-body glucose, lactate, and sodium tests were performed before the participant trial to monitor the performance of the biosensors (Figure 6C−E). Note, the initial potential drop in Figure 6E after participants entered the controlled environment chamber (see Supporting Information) occurred as the sensor reached a steady-state prior to cycling. These experiments display a similar trend for each lactate, glucose, and sodium biosensor in that the sensor response reached a relative plateau (taking variable amounts of time depending on sensor type) and increased upon cycling initiation. During these experiments and during the participant trial, separate microfluidic patches were worn simultaneously to collect sweat samples for external laboratory quantification of analytes (representing an average value of total sweat during the cycling trial). Gas chromatography mass spectrometry (GC-MS) was used to validate the glucose and lactate values in the sweat samples with the sensor output signal, while a commercial sodium assay kit was used to validate the sodium sensor response signal (see Supporting Information). These validation experiments were conducted during on-body cycling tests but before the participant trial, so that each sensor could be calibrated for improved accuracy during the participant trial as body movement and heat altered the sensor signals from those acquired previously *ex vivo*.

The glucose, lactate, and sodium concentration results of the 15-participant on-body sensor trial are exhibited in Figure 6B with placement of the sensors on the arm of each participant, as displayed in Figure 6A. In terms of a sensor development perspective, the results indicate that the sensor patch operated as intended with good adhesion throughout the test and continuous sweat flow to the sensor, which overall proves the efficacy of this LIG sensor/microfluidic patch in monitoring sweat glucose, lactate, and sodium levels in high stress environments. In general, the data from the 15-participant trial follows similar trends in which sweat concentrations of sodium, lactate, and glucose increase during physical exercise.[46,47] The data also demonstrate that participants have different sweat profiles as there is no noticeable correlation between the glucose, sodium, and lactate levels of participants with similar sex, age, weight, and fitness level. This data demonstrates that a baseline of nominal sweat analyte values needs to be developed on an individual basis and normal and abnormal sweat analyte concentration ranges cannot necessarily be applied broadly to patients. Moreover, one of the challenges associated with pinpointing sweat analyte correlations is the variability of sweat rate between individuals that skews studies that try to elucidate said correlations. For example, there is ambiguity between exercise intensity and sweat lactate levels as some reports demonstrate sweat lactate rising,[48−52] remaining level,[53] and even decreasing[54−58] in response to increased exercise intensity. One report explained that sweat lactate levels may decrease due to increasing exercise due to dilution as the speed of increasing sweat rate outpaces the increasing sweat lactate excretion rate.[57] Hence the sensor results could be improved in future work by including a real-time sweat rate sensor and correlating the response of each of the glucose, lactate, and sodium biosensor sweat rate. Nevertheless, the results presented herein are promising as they demonstrate how LIG created with a CO_2 laser that can be found ubiquitously across research universities and manufacturing facilities can be used with appropriate reagents to create reliable and accurate sweat analyte biosensors. Hence this work presents a sweat biosensor protocol that could be widely implemented to help decode the utility of sweat for medical diagnostics and real-time health monitoring.

CONCLUSION

In this work, we demonstrated the functionality of LIG as a flexible, wearable scaffold for enzyme attachment and selective polymer coating for use in perspiration sensing. LIG was formed via CO_2 laser processing of polyimide substrate, and laser carving parameters (speed, power, and frequency) were optimized for our lab. The graphene was characterized using XPS, Raman spectroscopy, SEM, and cyclic voltammetry,

https://doi.org/10.1021/acsami.3c04665
ACS Appl. Mater. Interfaces 2023, 15, 38201−38213

which described multilayer graphene with electrochemically active defects, similar to other described LIGs in the literature. Additionally, the electrochemical properties as measured in cyclic voltammograms of ferri/ferrocyanide compared well with other graphitic electrodes (average heterogeneous electron rate transfer coefficient over scan rates of 5−150 mV/s = 1.32×10^{-3} cm^2 s^{-1}, peak oxidation current ($i_{p,ox}$) of 2.35×10^{-5} A at 10 mV s^{-1}, ESA of 7.71×10^{-2} cm^2, ΔE_p of 82 mV at 10 mV s^{-1}). This process was then used to fabricate flexible 3- and 2-electrode devices which were tailored for selective and sensitive measurement of glucose, lactate, and sodium using specific coatings in each case. As prepared LIG sensors featured excellent performance in PBS and artificial perspiration, and interference from known physiological chemicals (uric acid, ascorbic acid, and chloride) remained negligible due to further surface modification with PPD. These sensors were incorporated into wearable, flexible tape/PET microfluidic patches, and on-body conditions were simulated using a custom perspiration pore field device attached to a syringe pump. Flowing tests in the wearable microfluidics proved the sensors' long-term robustness and response across the linear range of glucose, lactate, and sodium in human perspiration. Finally, the biosensors were tested in a 15-participant trial with results following similar reports of sweat concentrations of sodium, lactate, and glucose increasing during physical activity. The sensor results were validated with gold standard laboratory techniques, including GC-MS for glucose and lactate concentrations and a commercial assay kit for sodium.

Indeed, the results presented herein are promising as they demonstrate how LIG created with a CO_2 laser that can be found ubiquitously across research universities and manufacturing facilities can be used with appropriate reagents to create reliable and accurate sweat analyte biosensors. Hence this work presents a sweat biosensor protocol that could be widely implemented to help decode the utility of sweat for medical diagnostics and real-time health monitoring as the physiological mechanisms determining sweat composition are still not completely understood and published correlations between sweat and blood compositions are inconclusive.[47]

A major milestone of this work was that low-cost/scalable materials and manufacturing methods (LIG coupled with PET/tap microfluidics) could measure the average concentration of sweat glucose, lactate, and sodium levels during the 15-patient cycling tests, as validated with GC-MS for glucose and lactate and sodium with the assay kit. These LIG-based sensors were capable of monitoring sweat glucose, lactate, and sodium levels across the entire range in sweat without the need for preconcentration and even up to 32 mM for lactate, which is challenging to achieve due to the limitations of enzyme-based sensing ranges. However, improvements to the biosensors could be made to create a sensor system truly capable of accurate, nearly instantaneous sweat sensing. As mentioned previously, a real-time sweat rate sensor could be added to correlate the response of each of the glucose, lactate, and sodium biosensors to sweat rate and additionally an added pH sensor could be used to calibrate the sensors to pH differences that may occur between patients and during prolonged exercise regimes.[59] Moreover, to overcome the lack of sweat from those who are not sweating researchers have demonstrated that sweat can be chemically stimulated for hours using chemicals such as carbachol (half-life of 4−8 h).[60] Such a chemical stimulant could be applied to the skin sensor interface to induce a steady flow of sweat for analysis even when the patient is not exercising (not sweating).

Beyond sweat monitoring, the combination of these flexible and disposable LIG electrodes with microfluidics can be used to create cutting-edge sensing platforms. Such platforms have the potential for widespread implementation in lab-on-a-chip devices applied toward human and animal diagnostics, as well as environmental and food monitoring where small sample volumes and low-cost testing are vital for viable applications.[61] The continued use of LIG electrochemical sensors in tandem with microfluidics will pave the way for real time, continuous measurements of biochemical analytes, with new opportunities to provide accurate, personalized diagnostics in point of care locations outside medical offices, in field assessment of food safety, water quality analysis, and athletic performance.[62]

EXPERIMENTAL SECTION

Materials. Silver/silver chloride paste, polyphenelyenediamine (PPD), chloroplatinic acid hexahydrate, perchloric acid, ethyl-3-(3-dimethylaminopropyl) carbodiimide/*N*-hydroxysuccinimide (EDC/NHS), ferri-/ferrocyanide, PBS 10X, MES (4-morpholineethanesulfonic acid) buffer, sodium ionophore, sodium tetraphenylborate (NaTPB), poly(vinyl chloride) (PVC), bis(2-ethylhexyl) sebacate (DOS), tetrathiafulvalene (TTF), chitosan, acetic acid, glutaraldehyde, sodium chloride (NaCl), glucose, lactate, polyvinyl butyral (PVB), THF, acetone, ethanol, carbon nanotubes, and glucose oxidase were purchased from Sigma-Aldrich (Saint Louis, MO, USA). Lactate oxidase was acquired from Toyobo. Polyimide (Kapton) and poly(ethylene terephthalate) (PET) were purchased from McMaster-Carr (Elmhurst, IL, USA). Sodium assay kit (#K391-100) was purchased from BioVision (Waltham, MA, USA).

LIG Fabrication. LIG was fabricated in a similar fashion to previously published reports,[26,63] using a CO_2 laser (75W Fusion M2, EpilogLaser) to photonically anneal polyimide sheets (Dupont) and produce a porous, conductive graphene foam structure that forms as the result of rapid gas expansion. Different optimized settings for laser raster speed, power intensity, focal distance, and pulse frequency have been reported, indicating the need to find optimal parameters in each individual lab setting. In our experiments, a raster speed of 7, laser power of 7, pulse frequency of 50 (parameters defined by the laser software), and focal distance of 2 mm (offset of polyimide surface to laser focal plane) produced the most conductive, electrochemically active, and mechanically robust LIG. Additionally, a DPI (dots per inch) of 1200 in the drawing software (CorelDraw) used to send files to the laser cutter was necessary to obtain LIG with high electrical conductivity.

Prior to functionalization, LIG electrode leads were coated in silver paste (silver/silver chloride paste), and electrode stems were passivated with acrylic polish. Silver coating the leads increased the conductivity, provided a larger contact area for potentiostat clips to make electrical contact, and ensured no change in the sensor performance with repeated mechanical attachment. Passivating the stems prevented deposition on undesired areas of the electrode and fluid wicking through the LIG (causing leaks) during microfluidic testing. For the LIG counter electrode, the LIG was left bare, and for the LIG reference electrode, approximately half of the LIG was scratched off the polyimide substrate and the remaining LIG was coated with Ag/AgCl paste, covering the LIG up to the passivated stem.

LIG Functionalization. *GOx Sensors.* Platinum deposition on LIG working electrodes was carried out at a constant applied potential of −0.5 V in 2 mM chloroplatinic acid hexahydrate and 0.5 M perchloric acid for 30 s, removed and reinserted into the deposition solution to remove bubbles formed, and repeated for another 30 s following a similar procedure developed in our lab.[64] PPD was applied after platinum deposition via cyclic voltammetry for 40 cycles from 0 to 0.9 V at a scan rate of 20 mV s^{-1} in 5 mM PPD in 10X PBS following a similar method developed for a previously published

https://doi.org/10.1021/acsami.3c04665
ACS Appl. Mater. Interfaces 2023, 15, 38201−38213

glucose and ATP sensor.[33] Successful layer deposition was confirmed by an initial current peak at ∼0.4 V that diminished on successive scans as well as a visual darkening of the sensor surface post deposition. EDC/NHS covalent attachment was used to functionalize the LIG with GOx following previously demonstrated functionalization[15] with other biorecognition agents. EDC/NHS was used in a 0.4/0.1 M ratio in 0.1 M MES buffer (pH 6.0), and a small volume ∼5 μL was applied to the LIG and allowed to react for 90 min. The sensors were then rinsed in MES buffer followed by deposition of 1 μL of 4 wt %/vol enzyme in pH 7.4 PBS buffer and allowed to dry overnight in ambient conditions. Before testing, the sensors were washed thoroughly with PBS buffer to remove unbound enzyme and stabilize the sensor performance.

LOx Sensors. Fabrication of the LOx sensors followed an adapted method by Bandodkar et al.[6] LIG was first drop coated with 1 μL of 0.02 M TTF in acetone/ethanol (1:9 v/v), followed by a 2 μL drop coat of 60 mg/mL LOx in 0.25% vol/vol glutaraldehyde. Next, a coat of 2 μL of chitosan in 0.1 M acetic acid was drop coated and allowed to dry. An additional chitosan coat was achieved by dip-coating the sensor with the same chitosan solution. A final dipcoat of 3 wt % PVC in THF made up the final layer. The prepared sensors were dried in a refrigerator for 1 week before use.

Sodium Ion Selective Electrodes. Sodium ionophore, NaTPB, PVC, and DOS (1%, 0.55%, 33%, 65.45%) for a total mass of 100 mg were dissolved in 660 μL of THF and gently sonicated in an ultrasonic bath for ∼3 min to fully homogenize the ion selective membrane (ISM) in a procedure developed for previously reported potassium and ammonium ISM's.[65] ISM was applied to freshly prepared LIG working electrodes in 5 μL coats. Three coats were applied to avoid pinhole formation, and large bubbles were gently dissipated with a needle. As constructed ISEs were allowed to dry in fume hoods overnight, followed by conditioning in 1 mM NaCl for 24 h. LIG reference electrodes were made up of three layers on top of LIG: Ag/AgCl paste, CNT suspension, and PVB. First, a small amount of LIG was scratched off the polyimide and covered with Ag/AgCl. This layer dried for ∼20 min before drop coating 3 μL of 4 wt % CNT suspension in ethanol obtained by microtip probe sonication at amplitude 30% for 30 min. The CNT layer dried for ∼5 min, and then the PVB layer was applied in 3 coats of 3 μL, with brief drying of each layer between applications. Working and reference electrodes were conditioned in 1 mM NaCl (0.03%, 0.3%, and 1.0 mM) overnight before use.

Material Characterization. SEM images were taken using a FEI Quanta 250 FE-SEM (Thermo Fischer) at magnifications of 50, 150, and 500×. LIG samples were metal-sputter-coated prior to imaging. XPS measurements were performed by using a Kratos Amicus/ESCA 3400 instrument. The sample was irradiated with 240 W monochromated Mg Kα X-rays, and photoelectrons emitted at 0° from the surface normal were analyzed by using a DuPont type analyzer. Raman spectra of the LIG sample were directly obtained by a Horiba XploRA Plus confocal Raman microscope with a 532 nm laser operating at 1.2 mW. A 50× (0.5 NA) objective and a 600 grooves/mm grating to collect spectra from 100 to 3400 cm^{-1} with 30 s acquisition and 3 accumulations. Eighteen randomly selected locations were checked, and the average Raman spectra were plotted using SigmaPlot. Raman peaks were fitted to a Lorentzian function in Igor Pro 6.37 to calculate the I_D/I_G and I_{2D}/I_G ratios.

Electrochemical Testing. *Initial Electrochemical Sensor Characterization and Analyte Testing.* All electrochemical deposition steps were performed with an external liquid junction Ag/AgCl reference electrode, platinum wire counter electrode, and CHI electrochemical workstation (all CH Instruments Inc., Bee Cave, TX). All sensing tests excluding the microfluidic flowing experiments were conducted in stirred (300 rpm, 5 mm stirbar) 10 mL beakers. Cyclic voltammograms using ferri/ferrocyanide were performed using solutions of 5 mM ferri/ferrocyanide and 1 M KCl, with scan rates ranging from 10−150 mV/s, and potential windows of −0.1 to 0.6 V. A working potential for amperometric testing was set to 0.6 V for glucose sensors and 0.4 V for lactate sensors. Initial capacitive current drain was observed in all cases and was allowed to reach a stable plateau before addition of glucose or lactose were made. For ISEs, testing was performed in stirred beakers, and where noted, an external Ag/AgCl liquid reference electrode was used in place of the LIG reference electrode. Open circuit potential was used in full linear range tests, where the concentration of sodium was increased in 1-decade steps, and physiological range tests increased the concentration by 0.2 decade steps. All sensors were allowed to reach a stable potential before additions were made. Chronoamperometry was used to determine the potential stability of the ISEs based on a measurement of capacitance.[66] Using an external reference electrode and platinum wire counter electrode, 1 nA current was applied to the LIG SC-ISE working electrode for 60 s, and then the current was reversed in polarity for another 60s. The capacitance was calculated by the following equation, eq 2:

$$\text{potential drift} = \frac{\Delta E}{\Delta t} = i/C_L \tag{2}$$

where ΔE is the change in potential, Δt is the change in time, i is the applied current, and C_L is the low frequency−capacitance in μF.

Electrochemical impedance spectra were collected in 1 mM NaCl using conditioned ISEs in a frequency range of 1.5 MHz to 10 Hz with an AC amplitude of 0.005 V and a DC voltage of 0 V.

Electrochemical Sensing Procedure for Completed Devices. Once the sensors were fully fabricated, all electrochemical sensing was performed by using the LIG counter and reference electrodes. For microfluidic testing, solutions of artificial perspiration were prepared following DIN 53160-2 by mixing 1 g of urea and 5 g of NaCl in 1 L of DI water and adjusting the pH to 6.5 with added glucose, lactate, or sodium (for added sodium solutions, 5 g of NaCl was omitted) as noted.

Perspiration Pore Device Fabrication. 3D models of the perspiration pore device were designed in SolidWorks and 3D printed using a FormLabs Form3 printer. Figure 4A depicts the layer-by-layer configuration of the device. A perspiration pore layer was used to mimic sweat pores on skin. A grid of pores was lased using a CO_2 laser onto a thin sheet of polyimide with 100 μm holes spaced 100 μm apart in a 2 × 2″ grid. The perspiration pore layer was attached to the 3D printed base by using superglue and was then allowed to dry. The inlet tube connections were taped to the 3D printed part. Microfluidic tubing and fittings were installed, which minimized the volume in the system (∼350 μL), and a bubble trap (Darwin Microfluidics) was installed inline. The bubble trap mitigated bubble introduction into the sensing microfluidics, which was possible when changing syringes and could impact the sensor function and results. A syringe pump (Harvard Apparatus, Model 22) was used to power pressure driven flow at a constant rate of 1 mL h^{-1}.

Microfluidic Fabrication. Our microfluidic patch design follows similar published reports,[22] with one major caveat, we used a thin sheet of PET as the channel layer to circumvent leaking and inconsistent flow when using tape to define the channels. A blown-up view of the microfluidic assembly is shown in Figure 4A. The overall channel layout included smaller inlet channels feeding a larger central chamber (Figure 4B) that houses the working, reference, and counter electrodes, a design that has been demonstrated to improve the refreshing rate of changing of analyte concentration in perspiration in the sensing chamber. The PET sheet is marked with a crosshair to center the laser position, and then, the PET is cut to form channels using a CO_2 laser and computer designed 2D images. Next, a sheet of the same PET is fitted with medical grade double sided tape (3 M 1577) on both sides and adhered to the bottom of the channel layer. This stack is then brought back to the CO_2 laser, and the laser is centered on the crosshair again. A new image is used to control the laser's path, this time for the ring of circular inlets surrounding the sensing chamber, as these inlets need to interface directly with the skin/perspiration pore field. The final step in the microfluidic fabrication process is to cut a circular top layer composed of another tape/PET/tape stack, which is sealed to the inlet and channel layers. Fully functionalized LIG sensors are then adhered to the as constructed microfluidic patch to make the final top seal and to prepare the microfluidic sensor for testing. Sweat collection patches

https://doi.org/10.1021/acsami.3c04665
ACS Appl. Mater. Interfaces 2023, 15, 38201−38213

were also prepared for on-body studies to collect parallel sweat samples for off-body lab analysis, which followed the same fabrication procedure as the biosensing patches, except a sheet of PET was used in place of an LIG sensor to seal the top of the microfluidics.

Simulated Sweating Syringe Pump Testing. To validate sensor and microfluidic patch performance in a simulated sweating scenario, LIG/microfluidic devices were adhered to a custom sweat pore syringe pump device following previous reports.[67] This mount features pores of similar size and distribution as human skin, and the flow rate was controlled at 1 mL h^{-1} with a syringe pump. Experiments involving this setup were performed measuring the sensor's response to various concentrations of glucose/lactate/sodium spiked artificial sweat, and plateau values of current and potential were used to determine the sensor response to a given concentration of glucose, lactate, and sodium, respectively.

■ ASSOCIATED CONTENT

Supporting Information

The Supporting Information is available free of charge at https://pubs.acs.org/doi/10.1021/acsami.3c04665.

> Importance and benefits of real-time monitoring of sweat glucose, lactate, and electrolytes; on-body cycling trials; and sensor validation with gas chromatography mass spectrometry (GC-MS) and an assay kit (PDF)

■ AUTHOR INFORMATION

Corresponding Author

Jonathan C. Claussen − *Department of Mechanical Engineering, Iowa State University, Ames, Iowa 50011, United States;* orcid.org/0000-0001-7065-1077; Email: jcclauss@iastate.edu

Authors

Nate T. Garland − *Department of Mechanical Engineering, Iowa State University, Ames, Iowa 50011, United States;* orcid.org/0000-0003-1641-9861

Jacob Schmieder − *Department of Mechanical Engineering, Iowa State University, Ames, Iowa 50011, United States*

Zachary T. Johnson − *Department of Mechanical Engineering, Iowa State University, Ames, Iowa 50011, United States*

Robert G. Hjort − *Department of Mechanical Engineering, Iowa State University, Ames, Iowa 50011, United States;* orcid.org/0000-0003-2400-0710

Bolin Chen − *Department of Mechanical Engineering, Iowa State University, Ames, Iowa 50011, United States*

Cole Andersen − *Department of Mechanical Engineering, Iowa State University, Ames, Iowa 50011, United States*

Delaney Sanborn − *Department of Mechanical Engineering, Iowa State University, Ames, Iowa 50011, United States*

Gabriel Kjeldgaard − *Department of Mechanical Engineering, Iowa State University, Ames, Iowa 50011, United States*

Cicero C. Pola − *Department of Mechanical Engineering, Iowa State University, Ames, Iowa 50011, United States;* orcid.org/0000-0001-6141-9698

Jingzhe Li − *Department of Chemistry, Iowa State University, Ames, Iowa 50011, United States; The Ames Laboratory, U.S. Department of Energy, Ames, Iowa 50011, United States;* orcid.org/0000-0002-1856-1477

Carmen Gomes − *Department of Mechanical Engineering, Iowa State University, Ames, Iowa 50011, United States;* orcid.org/0000-0003-0095-6478

Emily A. Smith − *Department of Chemistry, Iowa State University, Ames, Iowa 50011, United States; The Ames Laboratory, U.S. Department of Energy, Ames, Iowa 50011, United States;* orcid.org/0000-0001-7438-7808

Hector Angus − *Department of Kinesiology, Iowa State University, Ames, Iowa 50011, United States*

Jacob Meyer − *Department of Kinesiology, Iowa State University, Ames, Iowa 50011, United States;* orcid.org/0000-0003-3180-5728

Complete contact information is available at: https://pubs.acs.org/10.1021/acsami.3c04665

Notes

The authors declare no competing financial interest.

■ ACKNOWLEDGMENTS

J.C.C. gratefully acknowledges funding support for this work by the Office of Naval Research under Award Number N000142012375, from the National Institute of Food and Agriculture, U.S. Department of Agriculture under Award Proposal Number 20216702134457, and from the National Science Foundation under Award Number CMMI-2037026 and NSF PFI-TT: 2141198.

■ REFERENCES

(1) Kim, J.; Campbell, A. S.; de Ávila, B.E.-F.; Wang, J. Wearable biosensors for healthcare monitoring. *Nat. Biotechnol.* **2019**, *37* (4), 389−406.

(2) Yang, Y.; Gao, W. Wearable and flexible electronics for continuous molecular monitoring. *Chem. Soc. Rev.* **2019**, *48* (6), 1465−1491.

(3) Bandodkar, A. J.; Wang, J. Non-invasive wearable electrochemical sensors: a review. *Trends Biotechnol.* **2014**, *32* (7), 363−371.

(4) Gao, W.; Emaminejad, S.; Nyein, H. Y. Y.; Challa, S.; Chen, K.; Peck, A.; Fahad, H. M.; Ota, H.; Shiraki, H.; Kiriya, D.; et al. Fully integrated wearable sensor arrays for multiplexed in situ perspiration analysis. *Nature* **2016**, *529* (7587), 509−514.

(5) Koh, A.; Kang, D.; Xue, Y.; Lee, S.; Pielak, R. M.; Kim, J.; Hwang, T.; Min, S.; Banks, A.; Bastien, P.; et al. A soft, wearable microfluidic device for the capture, storage, and colorimetric sensing of sweat. *Science Translational Medicine* **2016**, *8* (366), 366ra165−366ra165.

(6) Bandodkar, A. J.; Gutruf, P.; Choi, J.; Lee, K.; Sekine, Y.; Reeder, J. T.; Jeang, W. J.; Aranyosi, A. J.; Lee, S. P.; Model, J. B.; et al. Battery-free, skin-interfaced microfluidic/electronic systems for simultaneous electrochemical, colorimetric, and volumetric analysis of sweat. *Science Advances* **2019**, *5* (1), No. eaav3294.

(7) Choi, J.; Kang, D.; Han, S.; Kim, S. B.; Rogers, J. A. Thin, Soft, Skin-Mounted Microfluidic Networks with Capillary Bursting Valves for Chrono-Sampling of Sweat. *Adv. Healthcare Mater.* **2017**, *6* (5), 1601355.

(8) Karimi-Maleh, H.; Karimi, F.; Alizadeh, M.; Sanati, A. L. Electrochemical Sensors, a Bright Future in the Fabrication of Portable Kits in Analytical Systems. *Chem. Rec.* **2020**, *20* (7), 682−692.

(9) dos Santos, C. C.; Lucena, G. N.; Pinto, G. C.; Júnior, M. J.; Marques, R. F. C. Advances and current challenges in non-invasive wearable sensors and wearable biosensors—A mini-review. *MEDICAL DEVICES & SENSORS* **2021**, *4* (1), No. e10130.

(10) Padash, M.; Enz, C.; Carrara, S. Microfluidics by Additive Manufacturing for Wearable Biosensors: A Review. *Sensors* **2020**, *20* (15), 4236.

(11) Nyein, H. Y. Y.; Bariya, M.; Kivimäki, L.; Uusitalo, S.; Liaw, T. S.; Jansson, E.; Ahn, C. H.; Hangasky, J. A.; Zhao, J.; Lin, Y.; et al. Regional and correlative sweat analysis using high-throughput microfluidic sensing patches toward decoding sweat. *Science Advances* **2019**, *5* (8), No. eaaw9906.

(12) Shao, Y.; Wang, J.; Wu, H.; Liu, J.; Aksay, I. A.; Lin, Y. Graphene Based Electrochemical Sensors and Biosensors: A Review. *Electroanalysis* **2010**, *22* (10), 1027−1036.
(13) Liu, Z.; Tabakman, S.; Welsher, K.; Dai, H. Carbon nanotubes in biology and medicine: In vitro and in vivo detection, imaging and drug delivery. *Nano Research* **2009**, *2* (2), 85−120.
(14) He, Q.; Das, S. R.; Garland, N. T.; Jing, D.; Hondred, J. A.; Cargill, A. A.; Ding, S.; Karunakaran, C.; Claussen, J. C. Enabling Inkjet Printed Graphene for Ion Selective Electrodes with Postprint Thermal Annealing. *ACS Appl. Mater. Interfaces* **2017**, *9* (14), 12719−12727.
(15) Pola, C. C.; Rangnekar, S. V.; Sheets, R.; Szydłowska, B. M.; Downing, J. R.; Parate, K. W.; Wallace, S. G.; Tsai, D.; Hersam, M. C.; Gomes, C. L.; et al. Aerosol-jet-printed graphene electrochemical immunosensors for rapid and label-free detection of SARS-CoV-2 in saliva. *2D Materials* **2022**, *9* (3), 035016.
(16) Ye, R.; James, D. K.; Tour, J. M. Laser-Induced Graphene. *Acc. Chem. Res.* **2018**, *51* (7), 1609−1620.
(17) Behrent, A.; Griesche, C.; Sippel, P.; Baeumner, A. J. Process-property correlations in laser-induced graphene electrodes for electrochemical sensing. *Microchimica Acta* **2021**, *188* (5), 159.
(18) Garland, N. T.; McLamore, E. S.; Cavallaro, N. D.; Mendivelso-Perez, D.; Smith, E. A.; Jing, D.; Claussen, J. C. Flexible Laser-Induced Graphene for Nitrogen Sensing in Soil. *ACS Appl. Mater. Interfaces* **2018**, *10* (45), 39124−39133.
(19) Soares, R. R. A.; Hjort, R. G.; Pola, C. C.; Parate, K.; Reis, E. L.; Soares, N. F. F.; McLamore, E. S.; Claussen, J. C.; Gomes, C. L. Laser-Induced Graphene Electrochemical Immunosensors for Rapid and Label-Free Monitoring of Salmonella enterica in Chicken Broth. *ACS Sens.* **2020**, *5* (7), 1900−1911.
(20) Torrente-Rodríguez, R. M.; Lukas, H.; Tu, J.; Min, J.; Yang, Y.; Xu, C.; Rossiter, H. B.; Gao, W. SARS-CoV-2 RapidPlex: A Graphene-Based Multiplexed Telemedicine Platform for Rapid and Low-Cost COVID-19 Diagnosis and Monitoring. *Matter* **2020**, *3* (6), 1981−1998.
(21) Torrente-Rodríguez, R. M.; Tu, J.; Yang, Y.; Min, J.; Wang, M.; Song, Y.; Yu, Y.; Xu, C.; Ye, C.; IsHak, W. W.; et al. Investigation of Cortisol Dynamics in Human Sweat Using a Graphene-Based Wireless mHealth System. *Matter* **2020**, *2* (4), 921−937.
(22) Yang, Y.; Song, Y.; Bo, X.; Min, J.; Pak, O. S.; Zhu, L.; Wang, M.; Tu, J.; Kogan, A.; Zhang, H.; et al. A laser-engraved wearable sensor for sensitive detection of uric acid and tyrosine in sweat. *Nat. Biotechnol.* **2020**, *38* (2), 217−224.
(23) Xuan, X.; Kim, J. Y.; Hui, X.; Das, P. S.; Yoon, H. S.; Park, J.-Y. A highly stretchable and conductive 3D porous graphene metal nanocomposite based electrochemical-physiological hybrid biosensor. *Biosens. Bioelectron.* **2018**, *120*, 160−167.
(24) Bauer, M.; Wunderlich, L.; Weinzierl, F.; Lei, Y.; Duerkop, A.; Alshareef, H. N.; Baeumner, A. J. Electrochemical multi-analyte point-of-care perspiration sensors using on-chip three-dimensional graphene electrodes. *Anal. Bioanal. Chem.* **2021**, *413* (3), 763−777.
(25) Chen, B.; Johnson, Z. T.; Sanborn, D.; Hjort, R. G.; Garland, N. T.; Soares, R. R. A.; Van Belle, B.; Jared, N.; Li, J.; Jing, D.; et al. Tuning the Structure, Conductivity, and Wettability of Laser-Induced Graphene for Multiplexed Open Microfluidic Environmental Biosensing and Energy Storage Devices. *ACS Nano* **2022**, *16* (1), 15−28.
(26) Lin, J.; Peng, Z.; Liu, Y.; Ruiz-Zepeda, F.; Ye, R.; Samuel, E. L. G.; Yacaman, M. J.; Yakobson, B. I.; Tour, J. M. Laser-induced porous graphene films from commercial polymers. *Nat. Commun.* **2014**, *5* (1), 5714.
(27) Duy, L. X.; Peng, Z.; Li, Y.; Zhang, J.; Ji, Y.; Tour, J. M. Laser-induced graphene fibers. *Carbon* **2018**, *126*, 472−479.
(28) Ferrari, A. C. Raman spectroscopy of graphene and graphite: Disorder, electron−phonon coupling, doping and nonadiabatic effects. *Solid State Commun.* **2007**, *143* (1), 47−57.
(29) Ferrari, A. C.; Meyer, J. C.; Scardaci, V.; Casiraghi, C.; Lazzeri, M.; Mauri, F.; Piscanec, S.; Jiang, D.; Novoselov, K. S.; Roth, S.; et al. Raman Spectrum of Graphene and Graphene Layers. *Phys. Rev. Lett.* **2006**, *97* (18), 187401.
(30) Nguyen, V. T.; Le, H. D.; Nguyen, V. C.; Tam Ngo, T. T.; Le, D. Q.; Nguyen, X. N.; Phan, N. M. Synthesis of multi-layer graphene films on copper tape by atmospheric pressure chemical vapor deposition method. *Advances in Natural Sciences: Nanoscience and Nanotechnology* **2013**, *4* (3), 035012.
(31) McDermott, C. A.; Kneten, K. R.; McCreery, R. L. Electron Transfer Kinetics of Aquated Fe + 3/ + 2, Eu + 3/ + 2, and V + 3/ + 2 at Carbon Electrodes: Inner Sphere Catalysis by Surface Oxides. *J. Electrochem. Soc.* **1993**, *140* (9), 2593−2599.
(32) Bard, A. J.; Faulkner, L. R. *Electrochemical Methods: Fundamentals and Applications*; Wiley: 2000.
(33) Kucherenko, I. S.; Didukh, D. Y.; Soldatkin, O. O.; Soldatkin, A. P. Amperometric Biosensor System for Simultaneous Determination of Adenosine-5′-Triphosphate and Glucose. *Anal. Chem.* **2014**, *86* (11), 5455−5462.
(34) Claussen, J. C.; Kumar, A.; Jaroch, D. B.; Khawaja, M. H.; Hibbard, A. B.; Porterfield, D. M.; Fisher, T. S. Nanostructuring Platinum Nanoparticles on Multilayered Graphene Petal Nanosheets for Electrochemical Biosensing. *Adv. Funct. Mater.* **2012**, *22* (16), 3399−3405.
(35) Wu, H.; Wang, J.; Kang, X.; Wang, C.; Wang, D.; Liu, J.; Aksay, I. A.; Lin, Y. Glucose biosensor based on immobilization of glucose oxidase in platinum nanoparticles/graphene/chitosan nanocomposite film. *Talanta* **2009**, *80* (1), 403−406.
(36) Hojaiji, H.; Zhao, Y.; Gong, M. C.; Mallajosyula, M.; Tan, J.; Lin, H.; Hojaiji, A. M.; Lin, S.; Milla, C.; Madni, A. M.; et al. An autonomous wearable system for diurnal sweat biomarker data acquisition. *Lab Chip* **2020**, *20* (24), 4582−4591.
(37) Li, M.; Wang, L.; Liu, R.; Li, J.; Zhang, Q.; Shi, G.; Li, Y.; Hou, C.; Wang, H. A highly integrated sensing paper for wearable electrochemical sweat analysis. *Biosens. Bioelectron.* **2021**, *174*, 112828.
(38) Shitanda, I.; Mitsumoto, M.; Loew, N.; Yoshihara, Y.; Watanabe, H.; Mikawa, T.; Tsujimura, S.; Itagaki, M.; Motosuke, M. Continuous sweat lactate monitoring system with integrated screen-printed MgO-templated carbon-lactate oxidase biosensor and microfluidic sweat collector. *Electrochim. Acta* **2021**, *368*, 137620.
(39) Martín, A.; Kim, J.; Kurniawan, J. F.; Sempionatto, J. R.; Moreto, J. R.; Tang, G.; Campbell, A. S.; Shin, A.; Lee, M. Y.; Liu, X.; et al. Epidermal Microfluidic Electrochemical Detection System: Enhanced Sweat Sampling and Metabolite Detection. *ACS Sens.* **2017**, *2* (12), 1860−1868.
(40) Jia, W.; Bandodkar, A. J.; Valdés-Ramírez, G.; Windmiller, J. R.; Yang, Z.; Ramírez, J.; Chan, G.; Wang, J. Electrochemical Tattoo Biosensors for Real-Time Noninvasive Lactate Monitoring in Human Perspiration. *Analytical chemistry* **2013**, *85* (14), 6553−6560.
(41) Bobacka, J. Potential Stability of All-Solid-State Ion-Selective Electrodes Using Conducting Polymers as Ion-to-Electron Transducers. *Anal. Chem.* **1999**, *71* (21), 4932−4937.
(42) Hjort, R. G.; Soares, R. R. A.; Li, J.; Jing, D.; Hartfiel, L.; Chen, B.; Van Belle, B.; Soupir, M.; Smith, E.; McLamore, E.; et al. Hydrophobic laser-induced graphene potentiometric ion-selective electrodes for nitrate sensing. *Microchimica Acta* **2022**, *189* (3), 122.
(43) Radu, A.; Anastasova-Ivanova, S.; Paczosa-Bator, B.; Danielewski, M.; Bobacka, J.; Lewenstam, A.; Diamond, D. Diagnostic of functionality of polymer membrane − based ion selective electrodes by impedance spectroscopy. *Analytical Methods* **2010**, *2* (10), 1490−1498.
(44) Zamarayeva, A. M.; Yamamoto, N. A. D.; Toor, A.; Payne, M. E.; Woods, C.; Pister, V. I.; Khan, Y.; Evans, J. W.; Arias, A. C. Optimization of printed sensors to monitor sodium, ammonium, and lactate in sweat. *APL Materials* **2020**, *8*, 100905.
(45) U.S., J.; Rewatkar, P.; Goel, S. Miniaturized polymeric enzymatic biofuel cell with integrated microfluidic device and enhanced laser ablated bioelectrodes. *Int. J. Hydrogen Energy* **2021**, *46* (4), 3183−3192.
(46) Karpova, E. V.; Laptev, A. I.; Andreev, E. A.; Karyakina, E. E.; Karyakin, A. A. Relationship Between Sweat and Blood Lactate Levels

During Exhaustive Physical Exercise. *ChemElectroChem.* **2020**, *7* (1), 191−194.
(47) Klous, L.; de Ruiter, C. J.; Scherrer, S.; Gerrett, N.; Daanen, H. A. M. The (in) dependency of blood and sweat sodium, chloride, potassium, ammonia, lactate and glucose concentrations during submaximal exercise. *European Journal of Applied Physiology* **2021**, *121* (3), 803−816.
(48) Derbyshire, P. J.; Barr, H.; Davis, F.; Higson, S. P. J. Lactate in human sweat: a critical review of research to the present day. *Journal of Physiological Sciences* **2012**, *62* (6), 429−440.
(49) Pilardeau, P. A.; Chalumeau, M. T.; Harichaux, P.; Vasseur, P.; Vaysse, J.; Garnier, M. Effect of physical training on exercise induced sweating in men. *J. Sports Med. Phys. Fitness* **1988**, *28* (2), 176−180.
(50) Pilardeau, P. A.; Lavie, F.; Vaysse, J.; Garnier, M.; Harichaux, P.; Margo, J. N.; Chalumeau, M. T. Effect of different work-loads on sweat production and composition in man. *J. Sports Med. Phys. Fitness* **1988**, *28* (3), 247−252.
(51) Pilardeau, P.; Vaysse, J.; Garnier, M.; Joublin, M.; Valeri, L. Secretion of eccrine sweat glands during exercise. *Br J. Sports Med.* **1979**, *13* (3), 118−121.
(52) Mitsubayashi, K.; Suzuki, M.; Tamiya, E.; Karube, I. Analysis of metabolites in sweat as a measure of physical condition. *Anal. Chim. Acta* **1994**, *289* (1), 27−34.
(53) Fellmann, N.; Grizard, G.; Coudert, J. Human frontal sweat rate and lactate concentration during heat exposure and exercise. *J. Appl. Physiol Respir Environ. Exerc Physiol* **1983**, *54* (2), 355−360.
(54) Green, J. M.; Bishop, P. A.; Muir, I. H.; McLester, J. R., Jr.; Heath, H. E. Effects of high and low blood lactate concentrations on sweat lactate response. *Int. J. Sports Med.* **2000**, *21* (8), 556−560.
(55) Green, J. M.; Bishop, P. A.; Muir, I. H.; Lomax, R. G. Gender differences in sweat lactate. *Eur. J. Appl. Physiol* **2000**, *82* (3), 0230−0235.
(56) Green, J. M.; Bishop, P. A.; Muir, I. H.; Lomax, R. G. Lactate−Sweat Relationships in Younger and Middle-Aged Men. *Journal of Aging and Physical Activity* **2001**, *9* (1), 67−77.
(57) Buono, M. J.; Lee, N. V.; Miller, P. W. The relationship between exercise intensity and the sweat lactate excretion rate. *J. Physiol Sci.* **2010**, *60* (2), 103−107.
(58) Ament, W.; Huizenga, J. R.; Mook, G. A.; Gips, C. H.; Verkerke, G. J. Lactate and ammonia concentration in blood and sweat during incremental cycle ergometer exercise. *Int. J. Sports Med.* **1997**, *18* (01), 35−39.
(59) Brothers, M. C.; DeBrosse, M.; Grigsby, C. C.; Naik, R. R.; Hussain, S. M.; Heikenfeld, J.; Kim, S. S. Achievements and Challenges for Real-Time Sensing of Analytes in Sweat within Wearable Platforms. *Acc. Chem. Res.* **2019**, *52* (2), 297−306.
(60) Simmers, P.; Li, S. K.; Kasting, G.; Heikenfeld, J. Prolonged and localized sweat stimulation by iontophoretic delivery of the slowly-metabolized cholinergic agent carbachol. *Journal of Dermatological Science* **2018**, *89* (1), 40−51.
(61) Fernández-la-Villa, A.; Pozo-Ayuso, D. F.; Castaño-Álvarez, M. Microfluidics and electrochemistry: an emerging tandem for next-generation analytical microsystems. *Current Opinion in Electrochemistry* **2019**, *15*, 175−185.
(62) Zhu, J.; Huang, X.; Song, W. Physical and Chemical Sensors on the Basis of Laser-Induced Graphene: Mechanisms, Applications, and Perspectives. *ACS Nano* **2021**, *15* (12), 18708−18741.
(63) Nayak, P.; Kurra, N.; Xia, C.; Alshareef, H. N. Highly Efficient Laser Scribed Graphene Electrodes for On-Chip Electrochemical Sensing Applications. *Adv. Electron. Mater.* **2016**, *2* (10), 1600185.
(64) Johnson, Z. T.; Jared, N.; Peterson, J. K.; Li, J.; Smith, E. A.; Walper, S. A.; Hooe, S. L.; Breger, J. C.; Medintz, I. L.; Gomes, C.; et al. Enzymatic Laser-Induced Graphene Biosensor for Electrochemical Sensing of the Herbicide Glyphosate. *Global Challenges* **2022**, *6* (9), 2200057.
(65) Kucherenko, I. S.; Chen, B.; Johnson, Z.; Wilkins, A.; Sanborn, D.; Figueroa-Felix, N.; Mendivelso-Perez, D.; Smith, E. A.; Gomes, C.; Claussen, J. C. Laser-induced graphene electrodes for electrochemical ion sensing, pesticide monitoring, and water splitting. *Anal. Bioanal. Chem.* **2021**, *413* (25), 6201−6212.
(66) Bobacka, J. Potential Stability of All-Solid-State Ion-Selective Electrodes Using Conducting Polymers as Ion-to-Electron Transducers. *Analytical chemistry* **1999**, *71* (21), 4932−4937.
(67) Sato, K.; Sato, F. Individual variations in structure and function of human eccrine sweat gland. *American Journal of Physiology-Regulatory, Integrative and Comparative Physiology* **1983**, *245*, R203−R208.